# Nanoscale

Accepted Manuscript


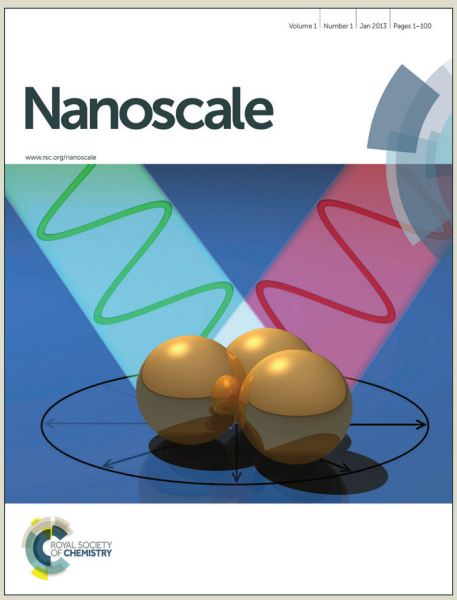





ROYAL SOCIETY OF CHEMISTRY

www.rsc.org/nanoscale

Cite this: DOI: 10.1039/c0xx00000x

www.rsc.org/xxxxxx

ARTICLE TYPE

# Rational design of a thermalresponsive-polymer-switchable FRET system for enhancing the temperature sensitivity of upconversion nanophosphors†

**Qingbo Xiao,[a] Yanfang Li,[a] jin Li,[a] Mengxin Zhang,[b] Zhijun Zhang,[b] and Hongzhen Lin,*[a]**

***Received (in XXX, XXX) Xth XXXXXXXXX 20XX, Accepted Xth XXXXXXXXX 20XX***
**DOI: 10.1039/b000000x**

Here we propose a thermoresponsive polymer PNIPAM modulated fluorescence resonance energy transfer (FRET) system to enhance the temperature sensitivity of upconversion nanophosphors (UCNPs). By utilizing red/near-infrared dual emitting $NaLuF_4$:$Mn^{2+}$,$Ln^{3+}$ ($Ln^{3+}$= $Yb^{3+}$, $Er^{3+}$, $Tm^{3+}$) UCNPs as energy donor and Au nanoparticles as acceptor, the temperature resolution of the UCNPs is significantly increased from 3.1 °C to 0.9 °C in the physiological temperature range. Conjugating the UCNPs and acceptors into discrete nanocomposites in our samples facilitates reversibly regulation of the emission intensity of UCNPs, which thus would extend their application range in biosensing, especially for probing the dynamic changes of local micro-environments in biological tissues. As there are a broad variety of stimuli to which smart polymers can reversibly response, our experiments are also extendable to various external conditions in local micro-environments, such as pH values, metal ions, glucose, and tissue-specific enzymes.

## 1. Introduction

Nanoscale temperature sensing in the physiological range (25-45 °C) is essential for understanding the dynamical behaviour and state of biosystems in modern biomedicine.[1] Recently, lanthanide ions ($Ln^{3+}$)-doped upconversion nanophosphors (UCNPs) are emerging as a new class of luminescent nanothermometers (NThMs) owing to their various advantages such as high resistance to photobleaching, low toxicity, and unique upconversion luminescence (UCL) properties upon near-infrared (NIR) excitation.[2-12] To date, a number of luminescent NThMs have been developed by exploiting the temperature dependent emission of $Ln^{3+}$ in upconverting and downconverting nanoparticles (NPs),[1,13-20] in which the common mechanism lying behind is that temperature influences the excited state population of $Ln^{3+}$ ions. However, such Boltzmann distribution governed mechanism sets an inherent limit on the temperature sensitivity of pristine UCNPs, thus most of the UCNPs-based NThMs (UC-NThMs) reported so far can only provide moderate temperature resolution. Recently, by preparing self-assembled hemispherical microstructures containing UCNPs and organic dye rhodamine 6G, better temperature sensitivity than the pristine UCNPs has been obtained by taking advantage of fluorescence resonance energy transfer (FRET) from UCNPs to rhodamine 6G.[13] This result reveals that constructing a FRET system to thermally modulate the UCL of UCNPs may be an effective way for enhancing the sensitivity of UC-NThMs. However, the FRET efficiency for the aforementioned UCNPs-dye system is significantly reduced in the solutions due to the highly dilution of dye molecules, which limits their practical application in biosystems. Compared to the separated donors and acceptors before (or after) detection procedure, conjugating the UCNPs and acceptors into discrete nanocomposites facilitates reversibly regulation of the FRET efficiency and the UCL intensity, which thus would extend their application range in biosensing, especially for probing the dynamic changes of local micro-environments in biological tissues. On the other hand, the UC-NThMs reported before mainly employed the short-wavelength visible UCL, which are susceptible to strong scattering in biological environments such as tissues. Due to the lack of efficient endogenous absorbers, the light scattering, absorbance and autofluorescence of tissues are minimum within the NIR (700-1100 nm) and red (600-700 nm) spectral range.[2-3,21-30] Therefore, tuning the output of UCNPs to maximize the red and NIR emission while minimize the short-wavelength emission is crucial for their deep tissue applications.

Compared to the methods of altering the spectral overlap or the relative dipole orientation, modulating the distance between donor and acceptor has been regarded as a general and facile way

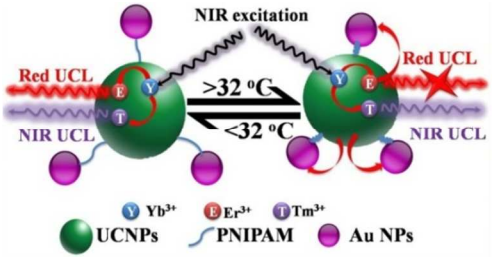


**Scheme 1.** Schematic illustration of smart-polymer-switchable FRET in upconverting nanocomposites.

for tuning the energy transfer efficiency in the FRET system [31]. Here, we describe a novel FRET switching method by employing the thermalresponsive polymer poly(N-isopropylacrylamide) (PNIPAM) as a spacer between the red/NIR dual emitting $NaLuF_4$: $Mn^{2+}$,$Ln^{3+}$ ($Ln^{3+}$= $Yb^{3+}$, $Er^{3+}$, $Tm^{3+}$) UCNPs donor and the Au nanoparticles (NPs) acceptor (Scheme 1). Specifically, the thermalresponsive-polymer-switchable FRET utilizes external stimuli-induced conformational changes, i.e., chain collapse/extension of PNIPAM to regulate the donor-acceptor distance and thus the UCL intensity dramatically and reversibly for an efficient luminescent sensing. PNIPAM undergoes a reversible phase transition from a hydrophilic, water-swollen state to a hydrophobic collapse state at its lower critical solution temperature (LCST, 32 $^oC$). It is thus anticipated that temperate change in the physiological range can be facilely read out from the UCL intensity variation of $NaLuF_4$: $Mn^{2+}$,$Ln^{3+}$ UCNPs. Noble metals such as Au and Ag NPs have been regarded as exceptionally sensitive antennas in modulating the optical properties of UCNPs due to strong surface plasmon resonance (SPR) absorption.[32-41] As a proof-of-concept demonstration, the Au NPs was employed as the energy acceptor in our system to thermally tune the UCL intensity of UCNPs via changing both the donor-acceptor distance and the SPR absorption of Au NPs as the variation of temperature, as the SPR absorption also vary with the thermoresponsive assembly/disassembly of metal NPs.[42] By ratiometric temperature sensing using red and NIR UCL of $NaLuF_4$:$Mn^{2+}$,$Ln^{3+}$ UCNPs, the experiments on UCNPs/PNIPAM/Au nanocomposites yield a relatively high temperature resolution of 0.9 $^oC$ as compared to that of 3.1 $^oC$ obtained from the pristine UCNPs.

## 2. Experimental Section

### 2.1 Materials

Oleic acid, amino-terminated PNIPAM (average $M_n$ 2500), 1-ethyl-3-(3-dimethyl aminopropyl) carboxylate (EDC) and *N*-hydroxysuccinimide (NHS) were purchased from Sigma-Aldrich Co. DMEM culture medium and fetal bovine serum (FBS) were purchased from Invitrogen. WST-1 was purchased from Biyuntian Biotechnology Institute.

### 2.2 Synthesis of $NaLuF_4$:$Mn^{2+}$,$Ln^{3+}$ UCNPs

Typically, x mmol $Tm(NO_3)_3$ ($0\leq x \leq 0.02$), (0.69-x) mmol $Lu(NO_3)_3$, 0.10 mmol $MnCl_2$, 0.20mmol $Yb(NO_3)_3$ and 0.01 mmol $Er(NO_3)_3$ dissolved in 5.0 mL deionized water was added to a mixture of NaOH (0.6 g), deionized water (4.0 mL), oleic acid (10.0 mL) and ethanol (20.0 mL) under thorough stirring. Then, 4.0 ml of deionized water contained 4.0 mmol of NaF was dropwise added to the mixture. After vigorous stirring at RT for 20 min, the colloidal solution were transferred into a 50 mL Teflon-lined autoclave, and subsequently heated at 200 °C for 10 h. After cooling to room temperature (RT), the obtained NPs were collected by centrifugation, washed with ethanol several times, and dried in vacuum overnight.

For comparison, $NaYF_4$:$Mn^{2+}$,$Ln^{3+}$ UCNPs were synthesized using the same procedure, except x mmol $Tm(NO_3)_3$ ($0\leq x \leq 0.02$), (0.74-x) mmol $Lu(NO_3)_3$ was replaced by 0.01 mmol $Tm(NO_3)_3$, 0.68 mmol $Y(NO_3)_3$. All of these as-prepared UCNPs could be easily redispersed in various nonpolar organic solvents such as cyclohexane, toluene, and chloroform.

### 2.3 Synthesis of MPA modified UCNPs

$NaLuF_4$:$Mn^{2+}$,$Ln^{3+}$ UCNPs (0.2 mmol) in 5 mL of cyclohexane was mixed with 1 mL of 3-mercaptopropionic acid (MPA) in 10 mL of ethanol and thorough stirred for 24 h. Then, the UCNPs were isolated by centrifugation, washed several times with deionized water and ethanol, and then redispersed in deionized water to form a transparent colloidal solution.

### 2.4 Synthesis of PNIPAM-conjugated UCNPs

Generally, 0.05 mmol MPA modified UCNPs was dissolve in 0.1 M phosphate-buffered saline (PBS) solution (pH 7.2) followed by the addition of 0.1 mmol EDC and 0.2 mmol NHS. The mixture was then stirred for 20 min to activate the carboxylic group of MPA. Subsequently, 0.2 g PNIPAM in PBS solution was added to the above solution, and the mixture was stirred overnight at RT. Excess EDC, NHS and PNIPAM were removed by washing with distilled water and ethanol several times. Finally, the PNIPAM coated UCNPs were dispersed in water.

### 2.5 Synthesis of Au NPs

Au NPs were prepared by citrate reduction of $HAuCl_4$ in the presence of citrate acid. Typically, 1 mL 1% (w/v) sodium citrate solution was added into a boiling solution of 30 mL 0.015% (w/v) $HAuCl_4$. After further boiling for 10 min, the heat source was removed and the dispersion was cooled down to RT.

### 2.6 Assembly of Au NPs with UCNPs

2 mg PNIPAM-conjugated UCNPs was dissolved in 2 mL deionized water, and then added quickly to 5 mL Au NPs solution under proper stirring and followed by sonication. The obtained UCNPs/PNIPAM/Au upconverting nanocomposites were purified several times in deionized water and redispersed in 1% (w/v) sodium citrate solution for measurement (2 mg/mL).

### 2.7 Cytotoxicity assay

WST assay was performed to evaluate the toxicity of the upconverting nanocomposites to human hepatocellular carcinoma (HepG2) cells. HepG2 cells were cultured in DMEM growth medium complemented with 10% FBS, streptomycin at 100 μg/mL and penicillin at 100 units/mL. The cells were maintained at 37 °C in a humidified atmosphere of 5% $CO_2$ in air. The cells were seeded into 96-well plates at cell density of $8\times10^3$ cells/well in 180 μL culture medium and maintained for 24 h. Then 20 μL of the upconverting nanocomposites with different concentrations was added to 96-well plates and incubated for another 24 h. Finally, the medium was replaced with 100 μL fresh DMEM, and 10 μL of WST-1 reagent was added to each well. After incubation for 1 h, the absorbance at 450 nm was determined by a standard microplate reader. All experiments were conducted in triplicate.

### 2.8 Characterization

Powder X-ray diffraction (XRD) patterns were collected using a BRUKER D8 Discover power diffractometer with Cu-Ka1 radiation (λ=0.154 nm). Both the low- and high-resolution transmission electron microscopy (TEM) measurements were performed using a Tecnai $G^2$ F20 S-Twin field-emission TEM

equipped with the energy-dispersive X-ray spectrum (EDS). Absorption spectra were recorded using PerkinElmer's Lamda 25 UV/vis spectrophotometer in the range of 190-1100 nm. Dynamic light scattering (DLS) experiments were carried out on an ALV-5000 spectrometer-goniometer equipped with an ALV/LSE-5004 light scattering electronic and multiple tau digital correlator and a JDS Uniphase He-Ne laser (632.8 nm) with an output power of 22 mW. UCL spectra were recorded on a Princeton Instruments (SP-2500i) spectrofluorimeter equipped with a 3W semiconductor laser (Inter-Diff Optoelectronics Technology Co., Ltd, Shanghai). The photos of upconversion luminescence were obtained digitally on a Nikon multiple CCD Camera. WST assay was conducted using a Biotek Elx 800 Microplate Reader. Cell lines were cultured in a water-jacketed $CO_2$ incubator (Thermo 3111).

The temperature variations for the solutions of the upconverting nanocomposites as well as PNIPAM-conjugated UCNPs were carried out by controlling the electric power dissipated by a resistor attached to the sample. The dispersions were stirred slowly during the measurements to obtain a uniform heat distribution. Each calibration consisted of five measurements in covered cuvettes. Spectra of samples were acquired in cuvettes which were heated from 25 to 55 °C under stirring.

## 3. Results and Discussion

### 3.1. Nanoparticle Characterization

The $NaLuF_4$:$Mn^{2+}$,$Ln^{3+}$ ($Ln^{3+}$=$Yb^{3+}$,$Er^{3+}$,$Tm^{3+}$) UCNPs were synthesized through a modified solvothermal strategy.[21] Codoping of $Mn^{2+}$ ions with $Ln^{3+}$ in UCNPs facilitates intense red and NIR UCL while minimize the short-wavelength emission due to the distinct energy transfer between $Mn^{2+}$ and $Ln^{3+}$ ions such as $Er^{3+}$ and $Tm^{3+}$.[21,26,30] To avoid possible formation of the impurity phase $NaMnF_3$, the $Mn^{2+}$ doping content was fixed to be a relatively low level of 10.0 mol% under current synthetic conditions. TEM image shows that the as-synthesized UCNPs are roughly cubic morphology with an average diameter of 25 ± 6 nm (Fig. 1a, c). The corresponding high-resolution TEM (HRTEM) image clearly demonstrates lattice fringes with an observed d-spacing of 0.30 nm (Fig. 1b), which is in good agreement with the lattice spacing for the (111) plane of cubic $NaLuF_4$. XRD pattern of the UCNPs can be exclusively indexed to cubic phase of $NaLuF_4$ crystals (JCPDS card No. 27-0725), which is consistent with TEM analysis of the samples (Fig. 1d). Composition analysis by EDS reveals the presence of Na, Lu, F, and doped $Mn^{2+}$, $Er^{3+}$, $Tm^{3+}$, $Yb^{3+}$ ions in the UCNPs (Fig. 1e). It is worth mentioning that all the $NaLuF_4$:$Mn^{2+}$,$Ln^{3+}$ UCNPs doped with different concentrations of $Tm^{3+}$ exhibit essentially the same crystal phase and morphology. Similarly, $NaYF_4$:$Mn^{2+}$,$Ln^{3+}$ UCNPs were also synthesized as control sample by the same method. TEM image shows the $NaYF_4$:$Mn^{2+}$,$Ln^{3+}$ UCNPs are also cubic in shape with a diameter of about 22 nm (Fig. S1, in the ESI†).

To obtain upconverting nanocomposites exhibiting tunable FRET interactions, amino-terminated PNIPAM were employed to tether UCNPs with Au NPs (Fig. 2a, Fig. S2a in the ESI†). Firstly, a ligand-exchange process was carried out by utilizing MPA to displace the original hydrophobic ligands of oleic acid on

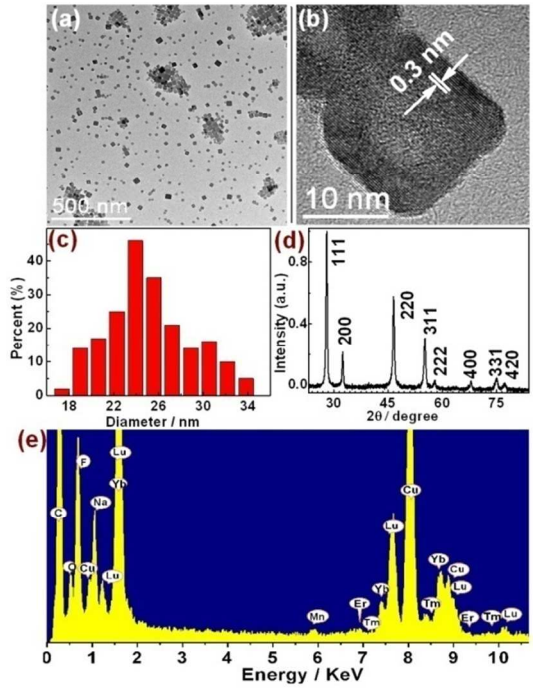


**Fig. 1.** (a) TEM, (b) HRTEM, (c) size distribution, (d) XRD pattern, and (e) EDS of $NaLuF_4$:$Mn^{2+}$,$Ln^{3+}$ UCNPs.

UCNPs surface. The sulfhydryl group (-SH) of MPA coordinates on the surface of the UCNPs, while the carboxy group (-COOH) stretches out, enabling the UCNPs to be readily dispersed in aqueous solution with typically negative surface charges. The -COOH on the surface of UCNPs allows further conjugation with amino-terminated PNIPAM by following the well established EDC/NHS protocol,[43-44] in which PNIPAM is covalently bounded to UCNPs through its amino group by using the cross-inking reagent EDC and NHS in PBS solution at RT. Finally, the PNIPAM-conjugated UCNPs were assembled with citrate stabilized Au NPs in aqueous solution via electrostatic interactions between the negatively charged citrate and the positively charged acylamino (-CO-NH-) of PNIPAM.[45] After being conjugated with PNIPAM, the UCNPs retain the morphological features of oleic acid capped UCNPs with only slight aggregation in water (Fig. 2b-c). The dynamic light scattering (DLS) measurement shows the particle size of PNIPAM-conjugated UCNPs (47 nm) is much larger than that of MPA modified UCNPs (25 nm), which is in agreement with the TEM analysis (Fig. S5 in the ESI†). The thicknesses of PNIPAM shells is estimated to be 1-2 nm, as can be seen clearly due to the different electron penetrability of the UCNPs cores and polymer shells. The surface functional groups of PNIPAM were further identified by the Fourier transform infrared (FTIR) spectroscopy (Fig. S3a in the ESI†). After the ligand-exchange process, a strong IR peak at 1639 $cm^{-1}$ was observed for the UCNPs, which is attributed to the C=O stretching mode of -COOH in MPA. In contrast to that of the MPA modified UCNPs, an abundant of new peaks are exclusively observed in the FTIR spectrum of PNIPAM-conjugated UCNPs. For example, peaks at 3299, 1648, and 1541 $cm^{-1}$ emerges in the FTIR spectrum, which are ascribed to the N-H, C=O and C-N stretching vibrations of PNIPAM, respectively. These findings confirm the successful conjugation of PNIPAM to the surface of UCNPs. Due to the existence of

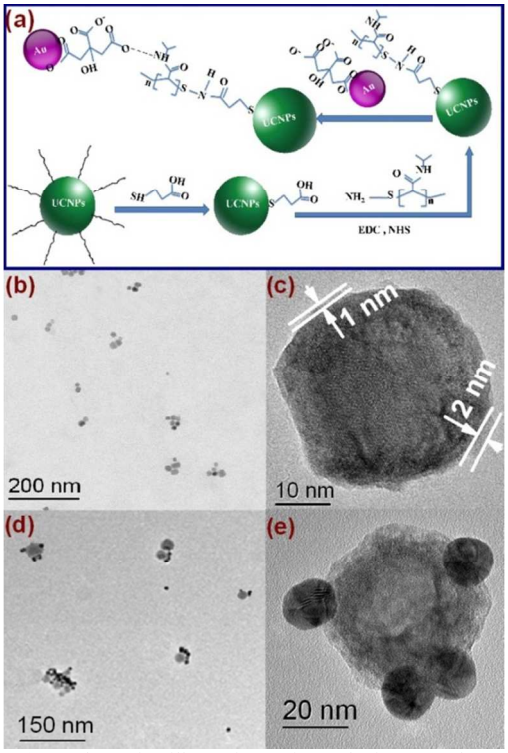


**Fig. 2.** (a) Schematic illustration of synthetic procedure of the upconverting nanocomposites. Low- and high-magnification TEM images of (b-c) PNIPAM-conjugated UCNPs and (d-e) the upconverting nanocomposites.

positively charged -CO-NH-, the Zeta-potential of PNIPAM-conjugated UCNPs was determined to be +30 mV at RT (Fig. S3b in the ESI†). On the other hand, the citrate-stabilized Au NPs possess a negative surface charge potential of -28 mV (Fig. S2b in the ESI†), which enables their electrostatic interaction with UCNPs in aqueous solution. As can be seen from the TEM images in Fig. 2d-e, Au NPs were firmly attached to the UCNPs, confirming the success formation of the UCNPs/PNIPAM/Au nanocomposites via the electrostatic interactions. A TEM image of a wide range of the upconverting nanocomposites in Fig. S4 in the ESI† shows there are approximately 2-4 Au NPs assembled with each of the $NaLuF_4$:$Mn^{2+}$,$Ln^{3+}$ NPs in the nanocomposites. Note that there was somewhat aggregation of the nanocomposites during TEM sample preparation, which was not obvious in solution according to the DLS measurements. The size response of the composites to temperature variation was further examined by DLS, which shows an average particle size of 61.2 nm at 25 $^{o}$C (Fig. S6 in the ESI†), consistent with the TEM analysis. The particle size of the upconverting nanocomposites reduces to 56.6 nm at 55 $^{o}$C. An abrupt increase of the hydrodynamic diameter can be seen as the temperature decrease from 37 to 31°C, reflecting occurrence of chain extension of PNIPAM within this temperature range. The mean diameter upon cycling above and below the LCST clearly shows that the chain collapse/extension behavior of PNIPAM in the upconverting nanocomposites is highly reversible, reflecting the great potential of modulating the distance between UCNPs and energy acceptors by utilizing smart polymers.

### 3.2. Upconversion Luminescence Properties

As can be seen in Fig. 3a, by introducing 10.0 mol% of $Mn^{2+}$ ions into $NaLuF_4$:$Ln^{3+}$ UCNPs, intense red and NIR emission bands centered at 660, 701 and 800 nm as well as weak green emission centered at 540 nm are observed upon excitation at 980 nm, which can be assigned to transitions of $^4F_{9/2}\rightarrow{}^4I_{15/2}$ ($Er^{3+}$), $^3F_3\rightarrow{}^3H_6$ ($Tm^{3+}$), $^3H_4\rightarrow{}^3H_6$ ($Tm^{3+}$) and $^2H_{11/2}$/$^4S_{3/2}\rightarrow{}^4I_{15/2}$ ($Er^{3+}$), respectively. Compared to $Mn^{2+}$-free sample, the red to green intensity ratio ($I_{Red}/I_{Green}$) of $NaLuF_4$: $Mn^{2+}$,$Ln^{3+}$ UCNPs significantly increases from 0.93 to 5.9 (Fig. S7 in the ESI), indicating the success of $Mn^{2+}$ in minimizing the short-wavelength emission of $Ln^{3+}$ ions. The increase of red emission intensity of the UCNPs by $Mn^{2+}$ can be attributed to nonradiative

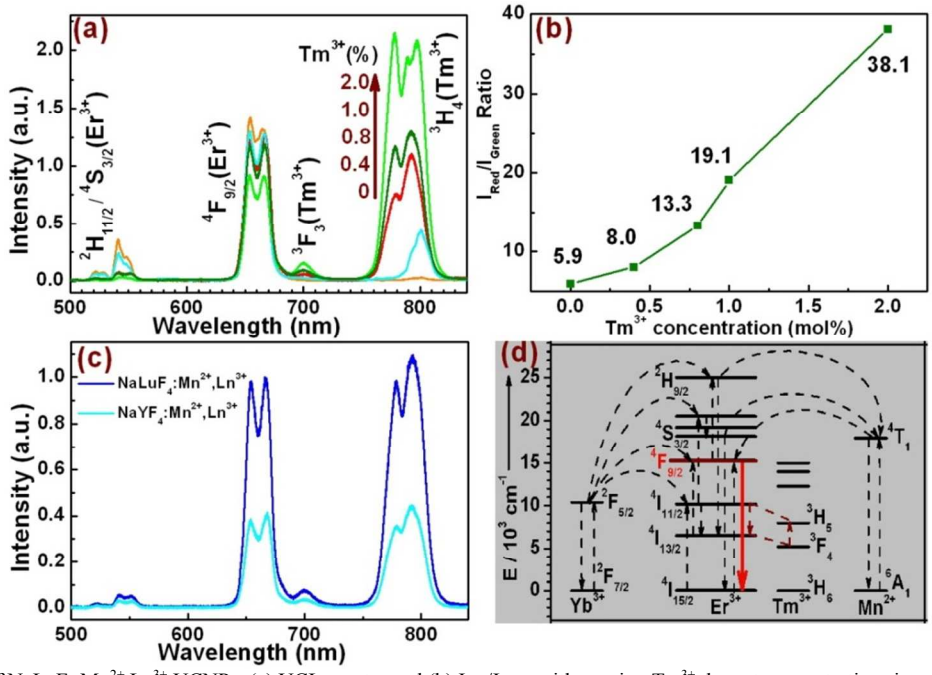


**Fig. 3.** UCL studies of $NaLuF_4$:$Mn^{2+}$,$Ln^{3+}$ UCNPs: (a) UCL spectra and (b) $I_{Red}/I_{Green}$ with varying $Tm^{3+}$ dopant concentrations in cyclohexane (1 mg/mL); (c) comparison of the UCL spectra with $NaYF_4$:$Mn^{2+}$,$Ln^{3+}$ UCNPs; (d) schematic energy level diagram showing the proposed UCL mechanisms of $Er^{3+}$.

energy transfer from the $^2H_{9/2}$ and $^4S_{3/2}$ levels of $Er^{3+}$ to the $^4T_1$ level of $Mn^{2+}$, followed by back transfer to the $^4F_{9/2}$ level of $Er^{3+}$ (Fig. 3d).[26] Except for $Mn^{2+}$, $Tm^{3+}$ ions are also found to change the transition possibilities of green and red emissions of $Er^{3+}$ in the UCNPs (Fig. 3a and b). As the $Tm^{3+}$ dopant concentration increase from 0 to 2.0 mol%, the $I_{Red}/I_{Green}$ ratio of $Er^{3+}$ significantly increases from 5.9 to 32.6, resulting in intense red and NIR UCL while the lack of short-wavelength UV and green emission. Thus, it is demonstrated that besides providing intense NIR emission at around 800 nm, the codoped $Tm^{3+}$ ions could also tune the color output of $Er^{3+}$ in $NaLuF_4$:$Mn^{2+}$,$Ln^{3+}$ UCNPs. In the current situation, the significant quenching effect of $Tm^{3+}$ ions for the green emission of $Er^{3+}$ is probably due to the depopulation of $^4I_{11/2}$ level of $Er^{3+}$ to the $^3H_5$ level of $Tm^{3+}$ (Fig. 3d).[46] The red emission intensity of $Er^{3+}$ slightly decrease with an increase of $Tm^{3+}$, which is presumably resulted from concentration quenching effect among the doped $Er^{3+}$ and $Tm^{3+}$ ions. To further reveal their optical properties, the UCL spectrum of $NaLuF_4$:$Mn^{2+}$,$Ln^{3+}$ UCNPs was compared with that of $NaYF_4$:$Mn^{2+}$,$Ln^{3+}$ with the same $Tm^{3+}$ concentration of 1.0 mol% (Fig. 3c). A more intense red/NIR dual emission can be observed for $Ln^{3+}$ in $NaLuF_4$ host, which is approximately three times of that in $NaYF_4$. Moreover, it is also found that the $I_{Red}/I_{Green}$ ratio of $Er^{3+}$ in $NaLuF_4$ host (19.1) is much larger than that in $NaYF_4$ (14.5), showing the superior property of $NaLuF_4$ host for intense red/NIR dual emission of $Ln^{3+}$.

The Au NPs possess a broad SPR absorption in the visible region, which matches well with the $^2H_{11/2}/^4S_{3/2}\rightarrow{}^4I_{15/2}$ and $^4F_{9/2}\rightarrow{}^4I_{15/2}$ transitions of $Er^{3+}$ (Fig. S8 in the ESI†). The absorption band of Au NPs is broadened and red shifted from around 519 nm to 538 nm after assembled with the UCNPs, due to the strong interparticle interaction and the coupling of the surface plasmon of neighboring Au NPs.[47] It can be seen that the absorption peak of Au NPs in the upconverting nanocomposites coincidently located in the green spectral region, which results in substantially intensity quenching for the $^2H_{11/2}/^4S_{3/2}\rightarrow{}^4I_{15/2}$ transitions of $Er^{3+}$, revealing the occurrence of efficient FRET from UCNPs to Au NPs. Besides drastic decline of the green emission intensity, the intensity of the red emission centered at 660 nm reduced by 14.2%, while the NIR emission centered at 800 nm was attenuated by only 9.3%. The existence of different FRET efficiencies for these emission bands demonstrates the capability of noble particles for tuning the intensity ratio of red to NIR emission in the upconverting nanocomposites.

### 3.3. Switchable FRET Detection of Temperature

To demonstrate the potential of the red/NIR dual emission upconverting nanocomposites as efficient UC-NThMs, the red and NIR emissions of the upconverting nanocomposites were investigated in the temperature range of 25-55 °C. To account for the heating affect of excitation source,[48-51] the temporal profile of temperature increase of the upconverting nanocomposites colloidal solution was recorded upon excitation at 980 nm to study the heat generation efficiency (Fig. S9 in the ESI†). It can be seen that the temperature of the solution rises to the maximum within 5 minutes, therefore the samples were all irradiated for at least 5 min before measurement to ensure a stable temperature. For probing local temperature in real biological systems, excitation light of 920 nm can be used instead to minimize the heating effect. As shown in Fig. 4a, the red emission of the upconverting nanocomposites drastically decreases by 47.1% as the environmental temperature increases from 25 to 55 °C. For comparison, only a moderate decrease of 22.8% was achieved for that of pristine UCNPs with merely PNIPAM coating (Fig. S10a in the ESI†), demonstrating the validity of the FRET system to modulate the UCL in the upconverting nanocomposites. To clarify the mechanisms that may responsible for the temperature responsive FRET system, the absorption of the upconverting nanocomposites were measured at 25 and 55 °C, respectively (Fig. 4a). The absorption band of Au NPs in the upconverting

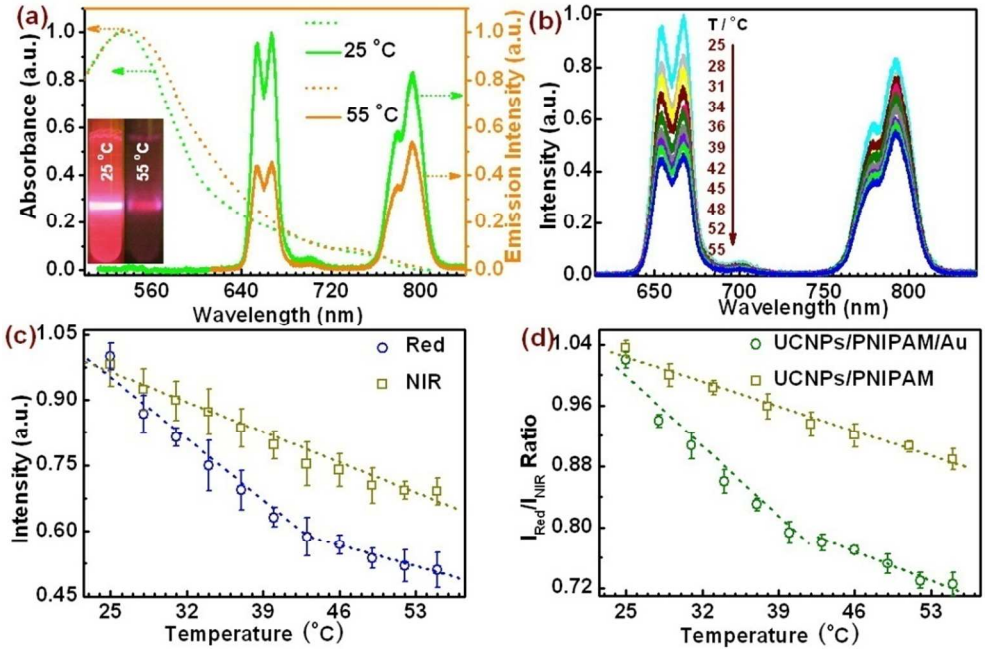


**Fig. 4.** Optical response of the upconverting nanocomposites to temperature variation: (a) absorption spectra, UCL spectra and corresponding luminescent photos of the colloidal solutions at 25 and 55 °C, respectively; (b) detailed UCL spectra at various temperature; (c) integrated intensity plots with the respective linear fits for the red and NIR emissions, respectively; (d) ratiometric calibration plots with the respective linear fits for the upconverting nanocomposites as well as PNIPAM-conjugated UCNPs.

**Table 1.** Temperature resolutions obtained with the upconverting nanocomposites and PNIPAM-conjugated UCNPs.

| | UCNPs/PNIPAM/Au | | | UCNPs/PNIPAM |
|---|---|---|---|---|
| UCL bands | Red | NIR | Red/NIR | Red/NIR |
| Uncertainty (%) | 5.4[a]/5.2[b] | 5.7 | 1.2[a]/1.5[b] | 1.4 |
| Resolution (°C) | 2.7[a]/7.1[b] | 5.8 | 0.9[a]/2.6[b] | 3.1 |

Temperature range: [a] 25-41 °C, [b] 44-55 °C.

nanocomposites further broaden and red shifted to 542 nm as the increase of temperature, which is assumed to be induced by the coupling of the SPR of neighboring Au NPs as the chain collapse of PNIPAM. Such spectral red shift increases the spectral overlap between the red emission of the UCNPs and the absorption of Au NPs, which results in further increase of FRET efficiency among them. Therefore, regulating the donor-acceptor distance by smart polymer spacer, together with tuning the spectral overlap, enables the red UCL of the UCNPs/PNIPAM/Au nanocomposites highly temperature sensitive.

To further calibrate the temperature sensitivity, the red and NIR emissions of the upconverting nanocomposites were carefully measured with a temperature increment of 3 °C. As can be seen in Fig. 4b, both the red and NIR emissions gradually decrease with increasing temperature, revealing that temperature can be accurately measured from the UCL intensities of the upconverting nanocomposites. The temperature-dependence of the red and NIR UCL is evident from the integrated areas of the $^4F_{9/2}\rightarrow{}^4I_{15/2}$ ($Er^{3+}$) and $^3H_4\rightarrow{}^3H_6$ ($Tm^{3+}$) transitions (Fig. 4c). The NIR emission decreases monotonously with the increase of temperature, which is similar to that of PNIPAM-conjugated UCNPs (Fig. S10b in the ESI†). In sharp contrast, two different regimes are clearly distinguishable for the red emission intensity of the upconverting nanocomposites, with a fast decrease within the temperature range of 25-41 °C, and a gentle slope at temperature above 41 °C. Such decrease for the red emission intensity of the upconverting nanocomposites is more apparent within a wider temperature range of 10-70 °C, as can be clearly seen in Fig. S11 in the ESI†. The appearance of the inflection for the red UCL at 25 and 41°C may reflect the occurrence of chain collapse/extension of PNIPAM at this temperature, which thus significantly regulated the FRET efficiency between UCNPs and Au NPs. The integrated intensity ratio of the red and NIR emissions ($I_{Red}/I_{NIR}$) for the upconverting nanocomposites as well as the PNIPAM-conjugated UCNPs were plotted versus temperature in Fig. 4d. Similar to the case of red UCL, the $I_{Red}/I_{NIR}$ of the upconverting nanocomposites exhibits a steeper slope within the temperature range of 25-41 °C and a slow decrease at temperature above 41 °C. As the ratio increment for $I_{Red}/I_{NIR}$ approximately follow linear relation with temperature in both regimes, thermal sensing based on these magnitudes would lead to constant resolutions. From the linear fitting, the fluorescence intensity decreases by 1.33 % per °C over the temperature range of 25–41 °C and 0.58% in the higher-temperature region. By defining the temperature resolution as the ratio between the standard deviation in the determination of the fluorescence intensity and the slope of the linear fit (fluorescence intensity decreased per °C) at a specific temperature,[15] the final thermal sensitivity can be obtained by careful analysis of the data included in Fig. 4c and d. Table 1 compared the averaged temperature resolution and the corresponding standard deviations obtained by the upconverting nanocomposites and PNIPAM-conjugated UCNPs. Owing to the successful elimination of the possible interferences to the UCL intensity, much lower standard deviations were obtained by using the ratiometric sensing. In our experimental conditions, a net uncertainty of 1.2-1.5% was determined for the $I_{Red}/I_{NIR}$ ratio within the temperature range of 25-55 °C, which results in high temperature resolutions as compared to that obtained from the red or NIR emission. Moreover, due to the presence of smart-polymer-switchable FRET, temperature resolution of 0.9 °C within 25-41 °C is obtained by the upconverting nanocomposites, which is much higher than that obtained from the PNIPAM-conjugated UCNPs (3.1 °C). Table 2 compares the temperature resolutions of some typical UC-NThMs as well as the NIR-to-NIR downconversion luminescent $LaF_3:Nd^{3+}$ NPs. It can be seen that the upconverting nanocomposites that we developed shows much larger temperature resolutions than most $Ln^{3+}$-doped NPs. It should be noted also that the $NaYF_4:Yb^{3+},Er^{3+}$ UCNPs exhibits a larger resolution than that of our work, but their short-wavelength green emission are susceptible to strong scattering in biological environments. We are firmly convinced that the temperature resolution could be further increased in our upconversion FRET system by increasing the FRET effect in the near future.

**Table 2.** Temperature resolutions obtained with $Ln^{3+}$-doped NPs.

| | Ratio of bands | Resolution | ref |
|---|---|---|---|
| $NaYF_4:Yb^{3+},Er^{3+}$ | $I_{523}/I_{541}$ | 0.45 | [15] |
| $NaYF_4:Yb^{3+},Ho^{3+}$ | $I_{541}/I_{656}$ | 7.3 | [15] |
| $NaYF_4:Yb^{3+},Tm^{3+}$ | $I_{475}/I_{695}$ | >20.0 | [15] |
| $LaF_3:Nd^{3+}$ | $I_{863}/I_{885}$ | 2 | [52] |
| nanocomposites | $I_{660}/I_{800}$ | 0.9 | this work |

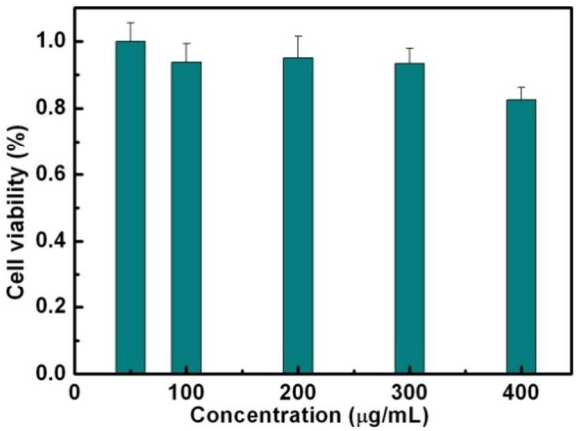


**Fig. 5.** *In vitro* cytotoxicity of the upconverting nanocomposites against HepG2 cell after 24 h incubation.

### 3.4. Cytotoxicity

For biosensing, it is critically important to evaluate the toxicity of

the obtained upconverting nanocomposites. Herein, the effect of the upconverting nanocomposites on cell proliferation was estimated with human hepatocellular carcinoma (HepG2) cells. The HepG2 cells were first grown with the medium containing different concentrations of the upconverting nanocomposites (0-400 μgmL$^{-1}$) for 24 h, and then the cell viability was determined on the basis of WST assay. The viability of untreated cells was assumed to be 100%. Upon incubation with the upconverting nanocomposites (200 μgmL$^{-1}$), only less than 7% of the HepG2 cells died (Fig. 5). Even at higher concentrations (400 μgmL$^{-1}$) of the upconverting nanocomposites, the cellular viabilities are estimated to be greater than 82%. These results indicate that the Moshchalkovprepared upconverting nanocomposites have low toxicity.

## 4. Conclusions

In summary, we have constructed a novel upconversion FRET system for high sensitivity temperature sensing by using thermoresponsive polymer PNIPAM as a spacer to regulate the distance between UCNPs donor and Au NPs acceptor. Intense red/NIR dual emission was obtained for $NaLuF_4$:$Mn^{2+}$,$Ln^{3+}$ UCNPs by codoping with $Mn^{2+}$. The intensity for red UCL of UCNPs/PNIPAM/Au nanocomposites was dramatically and reversibly regulated in response to temperature change. By the ratiometric sensing using the intensity ration of red to NIR emission, the upconverting nanocomposites yield a relatively high resolution of 0.9 °C in the physiological temperature range. Considering the broad variety of stimuli to which smart polymers can reversibly response, our method is extendable to probe the dynamic behavior of various external conditions in local micro-environments, such as pH values, metal ions, glucose, and tissue-specific enzymes.

## Notes and references

[a] *International Laboratory for Adaptive Bio-nanotechnology, Suzhou Institute of Nano-tech and Nano-bionics (SINANO), Chinese Academy of Science, Suzhou, 215123, China. E-mail: hzlin2010@sinano.ac.cn*
[b] *Suzhou Key Laboratory of Nanobiomedicine, Division of Nanobiomedicine, Suzhou Institute of Nano-tech and Nano-bionics, Chinese Academy of Sciences, Suzhou 215123, China.*

† Electronic Supplementary Information (ESI) available: [TEM image of $NaYF_4$:$Mn^{2+}$,$Ln^{3+}$ UCNPs, TEM and Zeta potential of Au NPs, FTIR spectrum and Zeta potential of PNIPAM-conjugated UCNPs, size distributions and multiple-run reversibility the upconverting nanocomposites to temperature variation, UCL spectrum of $NaLuF_4$: $Er^{3+}$,$Yb^{3+}$ UCNPs, and optical response of the PNIPAM-conjugated UCNPs to temperature variation.]. See DOI: 10.1039/b000000x/

1 X. D. Wang, O. S. Wolfbeis and R. J. Meier, *Chem. Soc. Rev.*, 2013, **42**, 7834-7869.
2 X. J. Xie, N. Y. Gao, R. R. Deng, Q. Sun, Q. H. Xu and X. G. Liu, *J. Am. Chem. Soc.*, 2013, **135**, 12608-12611.
3 Y. F. Wang, G. Y. Liu, L. D. Sun, J. W. Xiao, J. C. Zhou and C. H. Yan, *Acs Nano*, 2013, **7**, 7200-7206.
4 Y. S. Liu, D. T. Tu, H. M. Zhu, E. Ma and X. Y. Chen, *Nanoscale*, 2013, **5**, 1369-1384.
5 S. W. Hao, G. Y. Chen and C. H. Yang, *Theranostics*, 2013, **3**, 331-345.
6 J. Zhou, Z. Liu and F. Li, *Chem. Soc. Rev.*, 2012, **41**, 1323-1349.
7 Q. Q. Su, S. Y. Han, X. J. Xie, H. M. Zhu, H. Y. Chen, C. K. Chen, R. S. Liu, X. Y. Chen, F. Wang and X. G. Liu, *J. Am. Chem. Soc.*, 2012, **134**, 20849-20857.
8 G. F. Wang, Q. Peng and Y. D. Li, *Acc. Chem. Res.*, 2011, **44**, 322-332.
9 J. Hao, Y. Zhang and X. Wei, *Angew. Chem. Int. Edit.*, 2011, **50**, 6876-6880.
10 M. Haase and H. Schafer, *Angew. Chem. Int. Edit.*, 2011, **50**, 5808-5829.
11 F. Wang, Y. Han, C. S. Lim, Y. H. Lu, J. Wang, J. Xu, H. Y. Chen, C. Zhang, M. H. Hong and X. G. Liu, *Nature*, 2010, **463**, 1061-1065.
12 Z. J. Gu, L. Yan, G. Tian, S. J. Li, Z. F. Chai and Y. L. Zhao, *Adv. Mater.*, 2013, **25**, 3758-3779.
13 R. Chen, V. D. Ta, F. Xiao, Q. Y. Zhang and H. D. Sun, *Small*, 2013, **9**, 1052-1057.
14 D. Wawrzynczyk, A. Bednarkiewicz, M. Nyk, W. Strek and M. Samoc, *Nanoscale*, 2012, **4**, 6959-6961.
15 A. Sedlmeier, D. E. Achatz, L. H. Fischer, H. H. Gorris and O. S. Wolfbeis, *Nanoscale*, 2012, **4**, 7090-7096.
16 D. Jaque and F. Vetrone, *Nanoscale*, 2012, **4**, 4301-4326.
17 B. Dong, B. S. Cao, Y. Y. He, Z. Liu, Z. P. Li and Z. Q. Feng, *Adv. Mater.*, 2012, **24**, 1987-1993.
18 C. D. S. Brites, P. P. Lima, N. J. O. Silva, A. Millan, V. S. Amaral, F. Palacio and L. D. Carlos, *Nanoscale*, 2012, **4**, 4799-4829.
19 L. H. Fischer, G. S. Harms and O. S. Wolfbeis, *Angew. Chem. Int. Edit.*, 2011, **50**, 4546-4551.
20 F. Vetrone, R. Naccache, A. Zamarron, A. J. de la Fuente, F. Sanz-Rodriguez, L. M. Maestro, E. M. Rodriguez, D. Jaque, J. G. Sole and J. A. Capobianco, *Acs Nano*, 2010, **4**, 3254-3258.
21 G. Tian, Z. J. Gu, L. J. Zhou, W. Y. Yin, X. X. Liu, L. Yan, S. Jin, W. L. Ren, G. M. Xing, S. J. Li and Y. L. Zhao, *Adv. Mater.*, 2012, **24**, 1226-1231.
22 G. Chen, J. Shen, T. Y. Ohulchanskyy, N. J. Patel, A. Kutikov, Z. Li, J. Song, R. K. Pandey, H. Agren, P. N. Prasad and G. Han, *Acs Nano*, 2012, **6**, 8280-8287.
23 G. Chen, T. Y. Ohulchanskyy, S. Liu, W.-C. Law, F. Wu, M. T. Swihart, H. Agren and P. N. Prasad, *Acs Nano*, 2012, **6**, 2969-2977.
24 D. Q. Chen, Y. L. Yu, F. Huang, H. Lin, P. Huang, A. P. Yang, Z. X. Wang and Y. S. Wang, *J. Mater. Chem.*, 2012, **22**, 2632-2640.
25 H.-T. Wong, F. Vetrone, R. Naccache, H. L. W. Chan, J. Hao and J. A. Capobianco, *J. Mater. Chem.*, 2011, **21**, 16589-16596.
26 J. Wang, F. Wang, C. Wang, Z. Liu and X. G. Liu, *Angew. Chem. Int. Edit.*, 2011, **50**, 10369-10372.
27 G. Chen, T. Y. Ohulchanskyy, W. C. Law, H. Agren and P. N. Prasad, *Nanoscale*, 2011, **3**, 2003-2008.
28 J. Zhou, Y. Sun, X. Du, L. Xiong, H. Hu and F. Li, *Biomater.*, 2010, **31**, 3287-3295.
29 G. Y. Chen, T. Y. Ohulchanskyy, R. Kumar, H. Agren and P. N. Prasad, *Acs Nano*, 2010, **4**, 3163-3168.
30 M. Y. Xie, X. N. Peng, X. F. Fu, J. J. Zhang, G. L. Lia and X. F. Yu, *Scripta Mater.*, 2009, **60**, 190-193.
31 C. H. Li, J. M. Hu and S. Y. Liu, *Soft Matter*, 2012, **8**, 7096-7102.
32 W. Ge, X. R. Zhang, M. Liu, Z. W. Lei, R. J. Knize and Y. L. Lu, *Theranostics*, 2013, **3**, 282-288.
33 J. Zhang, B. Li, L. M. Zhang and H. Jiang, *Chem. Commun.*, 2012, **48**, 4860-4862.
34 Y. H. Wang, P. Shen, C. Y. Li, Y. Y. Wang and Z. H. Liu, *Anal. Chem.*, 2012, **84**, 1466-1473.
35 Z. Q. Li, L. M. Wang, Z. Y. Wang, X. H. Liu and Y. J. Xiong, *J. Phys. Chem. C*, 2011, **115**, 3291-3296.
36 S. Liu, G. Y. Chen, T. Y. Ohulchanskyy, M. T. Swihart and P. N. Prasad, *Theranostics*, 2013, **3**, 275-281.
37 W. Xu, S. Xu, Y. S. Zhu, T. Liu, X. Bai, B. A. Dong, L. Xu and H. W. Song, *Nanoscale*, 2012, **4**, 6971-6973.
38 I. M. Kennedy, L. Sudheendra, V. Ortalan, S. Dey and N. D. Browning, *Chem. Mater.*, 2011, **23**, 2987-2993.
39 W. Feng, L. D. Sun and C. H. Yan, *Chem. Commun.*, 2009, **29**, 4393-4395.
40 W. H. Zhang, F. Ding and S. Y. Chou, *Adv. Mater.*, 2012, **24**, Op236-Op241.
41 M. Saboktakin, X. C. Ye, S. J. Oh, S. H. Hong, A. T. Fafarman, U. K. Chettiar, N. Engheta, C. B. Murray and C. R. Kagan, *Acs Nano*, 2012, **6**, 8758-8766.
42 Y. D. Liu, X. G. Han, L. He and Y. D. Yin, *Angew. Chem. Int. Edit.*, 2012, **51**, 6373-6377.

43 L. Y. Wang, R. X. Yan, Z. Y. Hao, L. Wang, J. H. Zeng, H. Bao, X. Wang, Q. Peng and Y. D. Li, *Angew. Chem. Int. Edit.*, 2005, **44**, 6054-6057.

44 D. T. Tu, L. Q. Liu, Q. Ju, Y. S. Liu, H. M. Zhu, R. F. Li and X. Y. Chen, *Angew. Chem. Int. Edit.*, 2011, **50**, 6306-6310.

45 M. Karg, I. Pastoriza-Santos, J. Perez-Juste, T. Hellweg and L. M. Liz-Marzan, *Small*, 2007, **3**, 1222-1229.

46 E. M. Chan, G. Han, J. D. Goldberg, D. J. Gargas, A. D. Ostrowski, P. J. Schuck, B. E. Cohen and D. J. Milliron, *Nano Lett.*, 2012, **12**, 3839-3845.

47 S. Z. Zhang, L. D. Sun, H. Tian, Y. Liu, J. F. Wang and C. H. Yan, *Chem. Commun.*, 2009, **18**, 2547-2549.

48 L. M. Maestro, P. Haro-Gonzalez, B. del Rosal, J. Ramiro, A. J. Caamano, E. Carrasco, A. Juarranz, F. Sanz-Rodriguez, J. G. Sole and D. Jaque, *Nanoscale* **2013**, *5*, 7882- 7889.

49 A. Bednarkiewicz, D. Wawrzynczyk, M. Nyk and W. Strek, *Appl. Phys. B-Lasers O.* **2011**, *103*, 847-852.

50 A. K. Singh, S. Singh, D. Kumar, D. K. Rai, S. B. Rai and K. Kumar, *Opt. Lett.* **2012**, *37*, 776-778.

51 V. K. Tikhomirov, K. Driesen, V. D. Rodriguez, P. Gredin, M. Mortier and V. V. Moshchalkov *Opt. Express* **2009**, *17*, 11794-11798.

52 U. Rocha, C. Jacinto, W. F. Silva, I. Guedes, A. Benayas, L. M. Maestro, M. A. Elias, E. Bovero, F. C. J. M. van Veggel, J. A. G. Sole and D. Jaque, *Acs Nano*, 2013, **7**, 1188-1199.